Available online at www.sciencedirect.com
SCIENCE DIRECT®
PERGAMON
International Journal of Multiphase Flow 29 (2003) 813–840
International Journal of Multiphase Flow
www.elsevier.com/locate/ijmulflow

Droplets formation in turbulent mixing of two immiscible fluids in a new type of static mixer

T. Lemenand [a], D. Della Valle [b], Y. Zellouf [a], H. Peerhossaini [a,*]

[a] *Thermofluids and Complex Flows Research Group, Laboratoire de Thermocinétique CNRS UMR 6607, École Polytechnique de l'Université de Nantes, rue Christian Pauc, B.P. 50609, Nantes Cedex 3, 44306, France*
[b] *École Nationale d'Ingénieurs des Techniques des Industries Agricoles et Alimentaires, rue de la Géraudière, B.P. 82225, Nantes 44322, France*

Received 28 January 2002; received in revised form 29 January 2003

Abstract

The emulsification process in a static mixer high-efficiency vortex in turbulent flow is investigated. This new type of mixer generates coherent large-scale structures, enhancing momentum transfer in the bulk flow and hence providing favourable conditions for phase dispersion. The generation of the emulsion is described *via* a classical size-distribution function characterised by the Sauter diameter and a dispersion factor.

Keywords: Emulsification; Encapsulation; Dispersion; Granulometry; Optical microscopy; Sauter diameter; Size distribution; Static mixer; Two-phase flow

1. Introduction

The use of static mixers in the manufacture of emulsions or dispersions of immiscible fluids has received much attention over the last two decades thanks to recent progress in the hydrodynamics and the mixing performance of these systems. Process control and monitoring have been improved as well, especially in the chemical, petrochemical, food and cosmetics industries. Only a few manufacturers offer such equipment (Sulzer, Kenics, Optimix,...), however, and it is commonly agreed that novel hardware is greatly needed to handle specific new processes.

The objective of this study is to characterise the emulsification process achieved with a new static mixer commonly called HEV (high-efficiency vortex). The HEV design is based on curved

* Corresponding author. Tel.: +33-2-4068-3142; fax: +33-2-4068-3141.
E-mail address: hassan.peerhossaini@polytech.univ-nantes.fr (H. Peerhossaini).

0301-9322/03/$ - see front matter
doi:10.1016/S0301-9322(03)00032-6

baffles fixed on the tube walls that generate large-scale longitudinal vortices, substantially increasing transfer phenomena over those in the simple pipe. The study focuses on the granulometric characterisation of oil emulsions in water obtained with the static mixer HEV. The stability of the emulsions is obtained by encapsulating of the oil drops, and droplets are sized using optical microscopy. The mean size, size distribution, and power consumption are compared with those in some existing devices.

2. Scaling theory

Emulsions are heterogeneous systems formed by an immiscible liquid closely dispersed in another in droplet form. Significant input of mechanical energy is necessary to achieve the dispersion, only a small part of which is dedicated to the free energy gain. This energy is linked, in this case, to the interfacial area. If interfacial forces ($F_I = \sigma \cdot L$) derive from a potential E_I so that $F_I = dE_I/dn$ (with n the normal direction), then $E_I = \sigma \cdot A$ (A being the reference area). The addition of an emulsifier is useful to reduce the surface forces and facilitate drop breakup. Eventually, stabilisers and salts are used to reduce coalescence by repulsive electrical effects, but this step is not considered in the present study.

The size distribution (or granulometry) of the emulsions is described *via* a typical mean diameter based on statistical moments. The mean surface diameter or Sauter diameter, d_{32}, is the more relevant in cases where the interfacial area is a control parameter for the mass transfers or chemical reactions: it is used extensively in the characterisation of liquid/liquid or gas/liquid dispersions. Mathematical definition of the Sauter diameter is as following: $d_{32} = m_3/m_2$, m_q being the moment of order q for a probability density function $p(d)$

$$m_q = \int_{d_{\min}}^{d_{\max}} d^q p(d)\, dd \tag{1}$$

For any size distribution of discrete entities,

$$d_{32} = \frac{\sum_i n_i d_i^3}{\sum_i n_i d_i^2} \tag{2}$$

From Eq. (1), it is clear that the Sauter diameter depends both on $d_{\min}$, $d_{\max}$ and on the shape of the drop size distribution function.

A droplet subjected to mechanical stresses (pressure, velocity gradients, or turbulence forces) can burst into several droplets of lower size. This feature results from competitive effects between the rheological and interfacial properties of the two phases, and the flow conditions *via* mechanical forces.

Before droplet break up, the interface separating the continuous and the dispersed phase is deformed by the normal and tangential strains. The interfacial tension, σ, allows a spherical droplet of diameter d to withstand a stress as intense as the pressure difference from both sides of the interface, known as the Laplace pressure:

$$P_L = \frac{4\sigma}{d} \tag{3}$$

where σ is the interfacial tension and the spherical droplet has diameter d.

Since the break up undergoes a competition between external stress acting on the interface and the resistance of this interface, it can appropriately be characterised and quantified by a dimensionless Weber number, including or not the effect of the viscosity of the dispersed phase. A brief review of the models proposed for laminar and turbulent flows is given below.

2.1. Droplet breakup in laminar flow

According to Taylor (1932), droplet breakup in laminar shear flow is governed by the viscous shear stress $\tau = \mu_c \cdot \dot{\gamma}$, where $\dot{\gamma}$ is the shear strain and μ_c is the viscosity of the continuous phase. The droplet Weber number is then defined as

$$We_d = \frac{\mu_c \dot{\gamma} d}{4\sigma} \tag{4}$$

Taylor suggests that droplet break up occurs when the Weber number reaches a critical value We_{cr} (Schubert and Armbruster, 1992):

$$We_{cr} = \frac{\mu_c \dot{\gamma} d_{max}}{2\sigma} \tag{5}$$

The critical value can be used to determine the maximal droplet diameter d_{max} that can exist in a laminar shear field: Taylor (1934) has stated on theoretical ground that the droplet deformation is the ratio of viscous to interfacial tension forces, leading to a function of the viscosity ratio $R = \mu_d/\mu_c$ (of the dispersed and continuous phase viscosities, respectively), and of the droplet Weber number (Grace, 1982):

$$D_f = We_d \left(\frac{(19/16)R + 1}{R + 1} \right) \tag{6}$$

Following Grace's study of a single droplet in a simple shear flow, droplet break up can occur at a viscosity ratio more favourably in the range of $R = 0.1$–1, corresponding to a minimal value of We_{cr} (about 1) (Schubert and Armbruster, 1992). For lower values of this ratio (i.e. 0.01), a very high shear rate ($\dot{\gamma} \approx 10^6$–$10^7$ s^{-1}) is required to obtain small droplets ($d < 1$ μm) (Walstra, 1993). For higher values of R, the shear strain is less efficient to break up droplets; they behave like rigid spheres. If the viscosity ratio is above $R \approx 4$, no droplet division can occur, however large the shear rate.

The former analysis is also valid for the extensional laminar steady flows, in which the extensional rate $\dot{\varepsilon}$ is included in the definition of Weber number: $We_d = (\mu_c \dot{\varepsilon} d/4\sigma)$. For a R value about 1, the critical Weber number is close of 0.3, suggesting the better efficiency of the extensional flows at the same strain rate. The burst of droplet is no more limited by high values of R. The major feature of the extensional flows is that they are transient by nature, since it is not realistic to submit a single droplet to a constant strain rate during a "long" time. That is why a time scale analysis is required to predict the droplets burst, with respect to a relaxation time of the droplet, or the instabilities frequency.

2.2. Droplet breakup in turbulent flow

In turbulent flow, droplet break up occurs under the action of stresses arising from pressure fluctuations associated with the velocity fluctuations on the surface. These fluctuations occur on length scales of the order of the drop diameter. The theory of Kolmogorov and Hinze (Davies, 1985), based on the idea of energy cascade, is the main contribution to a physical understanding and is a universal model for droplet break up in turbulent flow. Kolmogorov theory is based on the concept that the energy contained in the large structures is transferred without dissipation to the smaller-scale structures, until dissipative scales are reached; at this stage kinetic energy is dissipated into heat under the effect of molecular viscosity. The Kolmogorov scale λ is characterised by a whirl Reynolds number of about unity:

$$\lambda \equiv v_c^{3/4}\varepsilon^{-1/4} \tag{7}$$

where v_c is the kinematic viscosity of the continuous phase and ε the energy dissipation per unit mass. The mean fluctuation velocity u' for eddies of size λ is then related to the local energy dissipation rate per unit mass of the fluid ε:

$$u' = (\varepsilon\lambda)^{1/3} \tag{8}$$

The size of the largest stable drop in the emulsion is determined by the equilibrium between the turbulent pressure fluctuations, which tend to deform and break up the drop, and the surface tension, which resists these deformations and holds the drop together. The ratio of these two constraints defines the droplet Weber number:

$$We_d = \frac{\rho_c u'^2 d}{\sigma} \tag{9}$$

where ρ_c is the density of the continuous phase. In homogeneous and isotropic turbulence, u' can be easily obtained from measurements (Pichot, 1984; Clark, 1988). More generally, in the inertial field for isotropic turbulence in the drop length scale, u' is given by:

$$u' = C_1\varepsilon^{1/3}d^{1/3} \tag{10}$$

where C_1 is a constant of order unity (Walstra, 1993). Hinze (1955) has suggested that, in homogeneous and isotropic turbulent flow, droplet break up occurs when the Weber number reaches a critical value We_{cr}. So the maximum diameter d_{max} of drops that resist further breakup by the eddies is obtained as:

$$d_{max} = C_2\varepsilon^{-0.4}\sigma^{0.6}\rho_c^{-0.6} \tag{11}$$

Eq. (11) is valid insofar as the drop size is controlled only by the mechanical divisions, i.e. in very diluted emulsions so that the coalescence can be neglected. This approach leads to the conclusion that the viscosity forces in the dispersed phase are negligible, what could be justified for drop sizes much larger than the Kolmogorov length scale.

The application of this model to "non-coalesced" systems was tested over a wide range of processes: stirred vessels, emulsifiers with ultrasound and homogenisers. Many authors report good prediction of the maximum droplet diameter, despite some discrepancies in the constant value.

Models reported in the literature preferentially use the Sauter diameter rather than the maximum diameter d_{max} of drops. Although size distributions depend on experimental conditions, a proportionality between the various average diameters and the maximum diameter is obtained experimentally, independently of the flow structure (Sprow, 1967),

$$\overline{d} = C_3 d_{max} \tag{12}$$

The basic formulation for liquid/liquid dispersions follows directly from the theory of Hinze–Kolmogorov (from Eqs. (11) and (12)). Actually, the velocity fluctuation in the range of d_{max} is estimated by $u' = (\varepsilon d_{max})^{1/3}$. Proceeding with the dimensional analysis for the mean dissipation rate, it is shown that for a stirred vessel the space-averaged dissipation rate is $\overline{\varepsilon} \propto (U^3/D)$, U and D being respectively the velocity scale (at the blade edge) and the size scale (impeller diameter), so that $u' = U(d_{max}/D)^{1/3}$. In addition, d_{max} follows from the critical Weber number:

$$\frac{d_{max}}{D} = \frac{We_{cr}}{\dfrac{\rho_c u'^2 D}{\sigma}}$$

Substituting u':

$$\left(\frac{d_{max}}{D}\right)^{5/3} = \frac{We_{cr}}{\dfrac{\rho_c U^2 D}{\sigma}}$$

gives the correlation of Shinnar (1961):

$$\frac{d_{max}}{D} = C_4 We^{-0.6} \tag{13}$$

with the scaling Weber number $We = (\rho_c U^2 D/\sigma)$.

The constant C_4, determined experimentally, depends on the geometry of the emulsifier and ranges between 0.09 and 0.15. This model was primarily developed for the case of stirred vessels, and was adapted to static mixers by Middleman (1974). The model developed to correlate droplet diameter takes into account the velocity dependence of the friction factor f in the pipes. Replacing $\overline{\varepsilon}$ in Eq. (10) as a function of the pressure drop by

$$\overline{\varepsilon} = \frac{U\Delta P}{\rho_c L} = \frac{fU^3}{2D}$$

yields

$$\frac{\overline{d}}{D} = C_5 We^{-0.6} f^{-0.4} \tag{14}$$

For a rectilinear cylindrical smooth pipe in a turbulent flow $f \sim Re^{-1/4}$, Eq. (14) becomes

$$\frac{\overline{d}}{D} = C_6 We^{-0.6} Re^{0.1} \tag{15}$$

The Streif formula (Streif, 1977) is slightly different from the previous theory for duct flows. After fitting the data to the Sulzer static mixer, the Sauter diameter is well predicted by:

$$\frac{d_{32}}{D_H} = C_{11} We^{-0.5} Re^{-0.15} \tag{16}$$

with the constant $C_{11} = 0.2$.

An other example of such fitting is found in the work of Poncelet and Neufeld (1996) in the study of the dispersive properties of static mixers:

$$\frac{\overline{d}}{D} = C_8 We^{-0.65} Re^{-0.2} \left(\frac{\mu_d}{\mu_c}\right)^{0.5} \tag{17}$$

The constant C_8 is given by experiments and depends on the geometry of the mixer. For Sulzer SMX and SMV mixers, C_8 is about 1.2.

Using Eq. (11), Davies (1985) adds a viscous stress term to the Laplace pressure as a resisting force:

$$d_{max} = C_9 \varepsilon^{-0.4} \left(\sigma + \frac{\mu_d u'}{4}\right)^{0.6} \rho_c^{-0.6} \tag{18}$$

Among the same lines, Calabrese et al. (1986) justified a corrective term for dilute emulsions taking into account the viscosity of the dispersed phase for applications in agitated tanks. For stirred tanks using Rushton impellers, they recommend:

$$\frac{d_{32}}{D_{agit}} = 0.054 \left[1 + 4.42 N_{vi} \left(\frac{d_{32}}{D_{agit}}\right)^{1/3}\right]^{0.6} We^{-0.6} \tag{19}$$

For a Kenics static mixer of pitch 1.5, Berkman and Calabrese (1988) report the following correlation:

$$\frac{d_{32}}{D_{agit}} = 0.49 \left[1 + 1.38 N_{vi} \left(\frac{d_{32}}{D_{agit}}\right)^{1/3}\right]^{0.6} We^{-0.6} \tag{20}$$

with the viscosity number

$$N_{vi} = \frac{\mu_d \cdot U}{\sigma} \left(\frac{\rho_c}{\rho_d}\right)^{0.5} \tag{21}$$

For the inviscid case, these models degenerate to a $We^{-0.6}$ behaviour. Measurements by Arai et al. (1977) and Wang and Calabrese (1986) show that the dispersed phase viscosity has negligible influence for viscosity ratios $\mu_d/\mu_c < 20$.

2.3. Effect of dispersed phase concentration

The models discussed above can predict the value of d_{max} only when the volume fraction of the dispersed phase is very low ($\phi < 0.05$). The value of the droplet mean diameter, and thus of interfacial area, is nevertheless modified by the volume fraction of the dispersed phase over 15 to 30%. Most recent work has suggested modifying the form of Eq. (13), to take into account the effect of the dispersed phase hold-up as follows:

$$\frac{d_{32}}{D} = C_9(1 + C_{10}\phi)We^{-0.6} \tag{22}$$

where the constant C_{10} is in the range 3–10 depending on the coalescence of the system. In stirred vessels, Pacek et al. (1998) have found $C_{10} = 22.8$. The authors attributed this very large value to the highly coalescent system used in their study (chlorobenzene/water).

In the same context, Lagisetty et al. (1986) use a modified expression for u' that depends on the dispersed phase hold-up ϕ, and then the equation for the Sauter drop diameter for Newtonian fluids in the limit of small viscosity becomes:

$$\frac{d_{32}}{D} = C_{11}(1 + C_{12}\phi)^{1.2}We^{-0.6} \tag{23}$$

For $C_{12} = 4$, the predictions of this model were found to be close to the experimental data of Coulaloglou and Tavlarides (1976).

The critical volume fraction over which the drop coalescence is important is not a universal value, but strongly depends on the fluids properties, especially the double electrical layer occurring at the interface.

3. Experimental apparatus and methods

3.1. Hydraulic loop

Two-phase flow experiments were performed using two immiscible fluid. The experimental setup consists of two similar feed loops, as shown in Fig. 1. Each loop consists of a tank

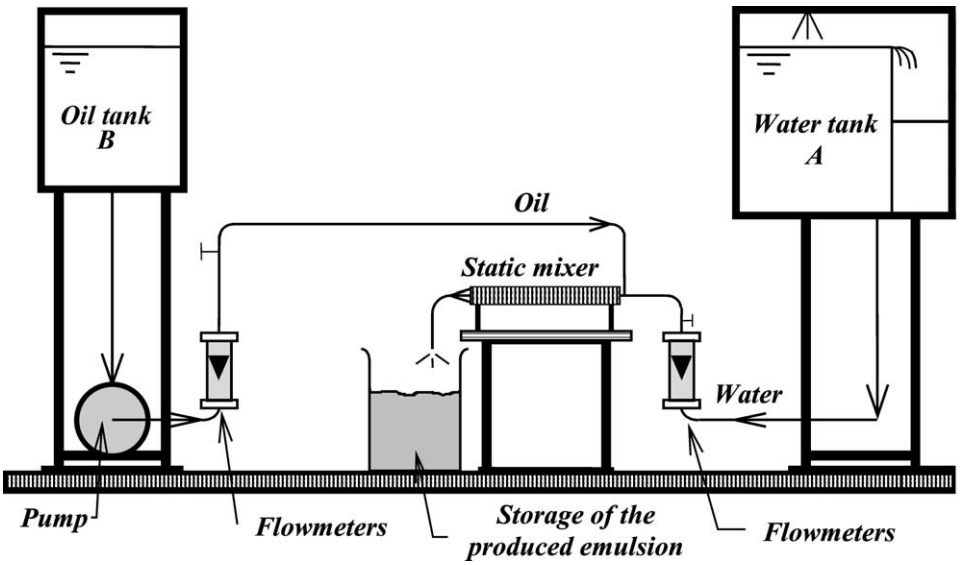

Fig. 1. Hydrodynamic loop for droplet formation in the HEV static mixer.

containing the working fluid. The oil is pumped with a centrifugal pump, while the water is supplied by a constant-level feed tank. The configuration with a free surface buffer tank avoids transmission of vibrations induced by the pump to the test section flow so as to reduce pseudo-turbulent fluctuations in the flow. The flow rates are controlled by valves and measured with two flowmeters with overlapping ranges.

3.2. Static mixer HEV

The geometry to be tested is a static mixer consisting of a straight tube of circular cross-section (inner diameter 20 mm) in which vortex generators are inserted. The geometry is shown schematically in Fig. 2. The vortex generators are small trapezoidal baffles that are fixed to the tube wall at a 30° angle: they are 7 mm long, and 7 and 5 mm at the bases, respectively on the wall and at the end of the trapezoid. The hydraulic diameter, D_H, is found to be 17.1 mm.

The role of the baffles in the test section is to generate longitudinal vortices that intensify turbulence and thus decrease the characteristic length of micro-mixing. In Fig. 3, these vortices are visualised by the laser-induced fluorescence (LIF) technique, in the case of transitional Reynolds number ($Re = 1500$). Indeed, flow visualisation is not effective in turbulent flow because of the very quick mixing of the fluorescent component. The flow structures shown on Fig. 3 are qualitatively representing the flow pattern at high Reynolds numbers too. The mushroom-shaped vortices visible in the cross-section are enhanced as Reynolds number increases. Four pairs of vortices are generated at each section and the succession of baffles along the longitudinal axis of the static mixer creates a complex whirl combination. Detailed information on the flow pattern and turbulence structure of single-phase flow in the static mixer can be found in Mokrani et al. (1995).

3.3. Working fluids

The working fluids are water for the continuous phase, and a technical vaseline oil without any additive for the dispersed phase. The set-up allows running experiments corresponding to dispersed-phase mixing rates of up to 15%, with Reynolds numbers ranging from 7500 to 15 000. The physical properties of this oil loaded with 10% volume of encapsulation reactant (see Section 3.4) are presented in Table 1.

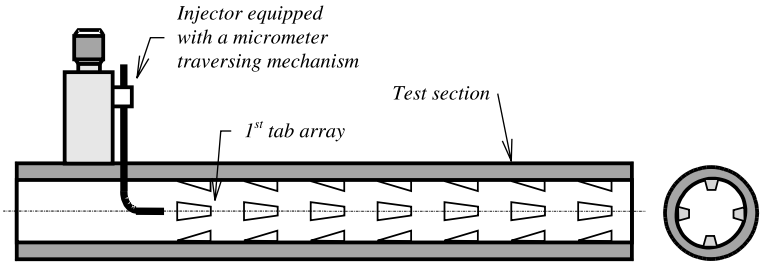

Fig. 2. Details of the test section geometry and injection device for two-phase flow experiments.

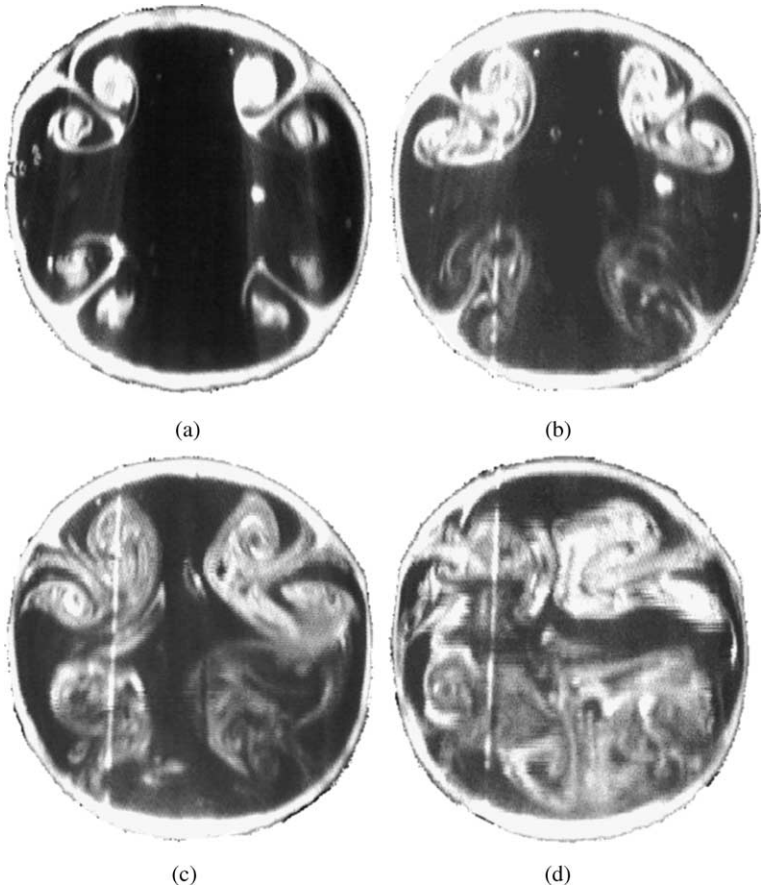

Fig. 3. Photographs of the cross-section of longitudinal vortices downstream of (a) first, (b) second, (c) third and (d) fourth baffle array for $Re = 1500$.

Table 1
Physical properties of oil with 10% vol. of hexamethylene diisocyanate

Property (20 °C)	Value	Measurement methods
Kinematic viscosity	30×10^{-6} m^2 s^{-1}	Mettler™ RM180 rheometer
Density	0.85	Data Technical™
Interfacial tension with water	20×10^{-3} N m^{-1}	Krüss™ tensiometer (K12) by the ring method

3.4. Micro-encapsulation technique for liquid–liquid flow investigation

Since the emulsion of water and oil is naturally unstable, coalescence phenomena will occur at the exit of the HEV. The droplet statistics may then change significantly before they can be sized,

so that the droplet measurements may not represent the emulsion obtained by the HEV. In order to fix the droplet size and avoid their coalescence, a micro-encapsulation operation was performed on the emulsion at the exit from the test section.

The process used here is based on the isocyanate-amine polymerisation reaction (monomers). A 10% volume fraction of hexamethylene diisocyanate ($OCN(CH_2)NCO$) is added to the oil in the feeding tank. As the dispersion production is continuous, a sample is rapidly removed into a flask containing 50 ml of demineralised water and 5.6 ml of ethylene diamine ($NH_2CH_2CH_2NH_2$) and is gently stirred at the optimal temperature of 65 °C. The polymerisation reaction occurs at the interface of the two phases, encapsulating the droplets with a rigid polymer film.

Morançais (1997) has shown that the size distribution is not affected by this encapsulation method, and moreover that the granulometry of the dispersion remains unchanged for at least one week.

3.5. Droplet diameter measurement

Using light scattering for automatic droplet sizing was not convenient in the present case, because of the formation of numerous polymer aggregates due to the reagents during encapsulation. However, optical methods were shown to sort the droplets efficiently, and hence, emulsions were visualised by optical microscopy.

A video-optic computer-assisted device was used for the granulometric analysis. It is composed of an optical microscope of binocular type that allows 126X enlargement and a colour CCD camera, which sends a signal to an acquisition card that allows obtaining of digitised frames stored in a standard personal computer.

The software with a pointer mouse was used to measure oil drop diameters directly on the monitor, by a two-point technique. A visual trace on the monitor lets one avoid counting the diameter of the same droplet more than once. Fig. 4 shows some photographs of various sampled dispersions.

Since the measurements of droplet diameter are based on sampling a large number of experiments, it is crucial to determine the population (number of droplets) of the samples so that the diameter distribution is independent of the population. The empirical method used here entailed measuring the distance between two distributions obtained by analysis of two populations, the

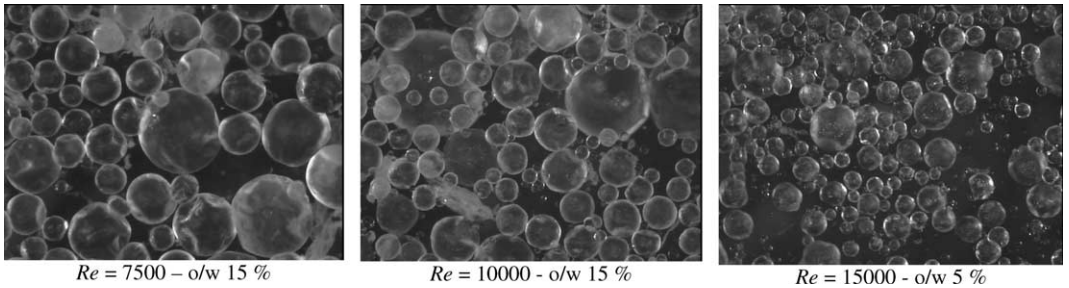

Fig. 4. Droplet samples processed by the software.

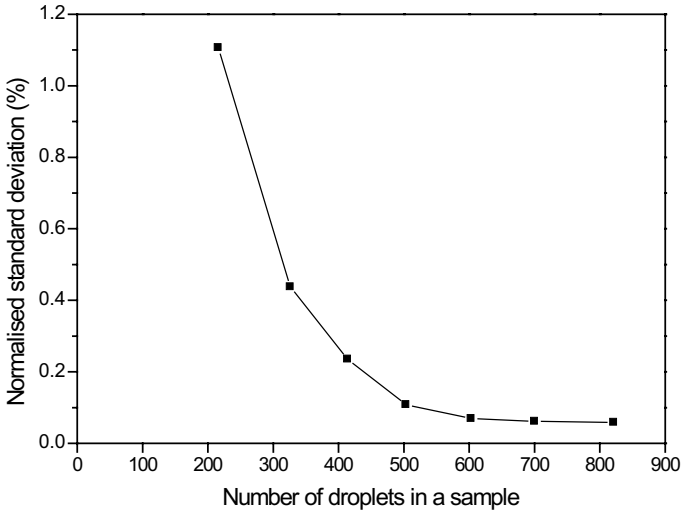

Fig. 5. Average standard deviation according to the population sample.

second one built from the first by increasing the drop population. The distance (or residual) is evaluated by a normalised standard deviation, defined by

$$\mathrm{SD}_n = \frac{\sum_i (f_i - f_i')^2}{N_\mathrm{c}} \tag{24}$$

where f_i and f_i' are the droplet frequencies (of the same class diameter, d_i) for two successive distributions and N_c is the class number. Fig. 5 plots this gap between two successive distributions as a function of the number of droplets of the sample. It can be seen that beyond 600 droplets this value stabilises at the global accuracy of the measurement. Henceforth, this minimal number of 600 is retained for droplet diameter measurement. It is important to note that all the droplets in a view are numbered, and that a sample may consist of several views.

Fig. 6 shows two examples of the size frequency distribution, using linear diameter classes. However, it was more appropriate, for this study, to use the volume distribution function versus logarithmic diameter classes.

3.6. Reproducibility and procedure sensitivity

A test was carried out to check the effect of a new operator and of a new trial on the measured characteristics of the final emulsion produced by the static mixer HEV. Nominal operating conditions were at Reynolds number $Re = 10\,000$ and internal phase concentration $\alpha = 15\%$: two operators (I and II) on different days (1 and 2) attempted to reproduce the same experiment, and the resulting size distributions were compared. The two Sauter mean diameters d_{32} and the standard deviation of the diameters SD differed by less than 5%. This good global reproducibility can be observed in Fig. 7.

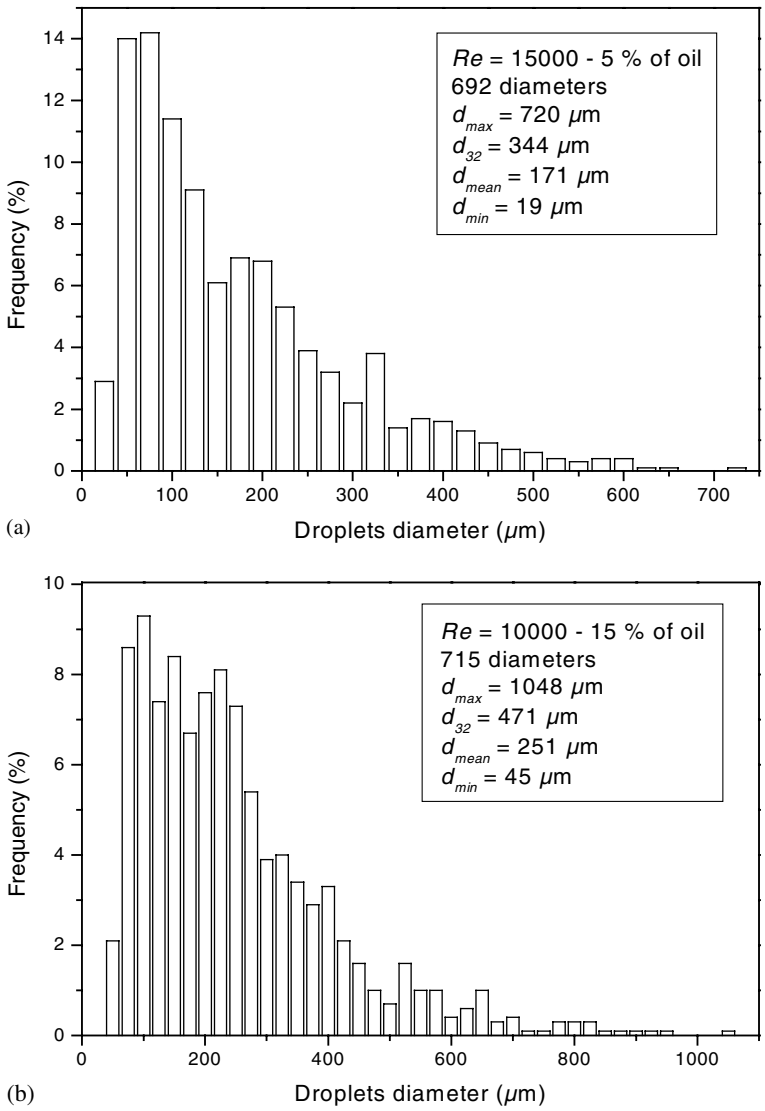

Fig. 6. Granulometric distribution of droplets (a) $Re = 15000$, 5% oil (b) $Re = 10000$, 15% oil.

4. Results

4.1. Experimental plan

In emulsification processes using static mixers for a given geometry, both the continuous phase flow rate and the dispersed phase flow rate determine the hydrodynamics of the problem. The total flow rate is the arithmetic sum of both volume flow rates

$$Q_T = Q_{water} + Q_{oil} \tag{25}$$

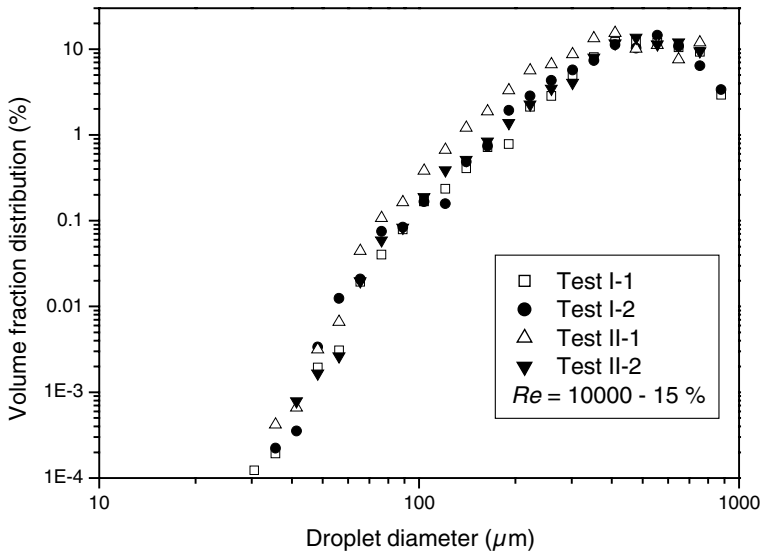

Fig. 7. Granulometric distribution obtained by microscope analysis; test of reproducibility and procedure sensitivity.

The superficial velocity in the system is defined with Q_T

$$U = \frac{Q_T}{\pi \frac{D^2}{4}} = \frac{Q_{water} + Q_{oil}}{\pi \frac{D^2}{4}} \tag{26}$$

where D is the reactor mean diameter (the volume occupied by the baffles is neglected). Assuming that there is no slip velocity between the two phases (this was checked with the pressure gradient), the internal phase concentration Φ is defined by

$$\Phi = \frac{Q_{oil}}{Q_{water} + Q_{oil}} \tag{27}$$

Hence, the superficial velocity can be expressed by

$$U = \frac{Q_{oil}}{\Phi \pi \frac{D^2}{4}} = \frac{Q_{water}}{(1-\Phi)\pi \frac{D^2}{4}} \tag{28}$$

In the present study, the objective is to investigate the effect of the Weber number on the bead distribution. The Weber number could be varied either through the physical properties of the fluids, i.e. the density and the interfacial tension, or the hydrodynamic conditions. However the density can not be significantly modified for a system of given fluids. The interfacial tension could easily be changed *via* the adjunction of surfactants but these components strongly interact with the encapsulation process. As a consequence the flow rate remains the only parameter allowing us to cover a large Weber number range.

The working range of the dispersed volume fraction is relatively low (the upper bound is 15%), so that the turbulent characteristics of the continuous phase prevail in the dispersion mechanism. Hence, at given hold-up in the range 0–15%, four total flow rate values were fixed (four given Reynolds numbers, since fluids and the geometry are unchanged) in order to obtain similar

Table 2
Operating conditions

Re	Φ (%)	U (m s^{-1})	Q_{water} (l s^{-1})	Q_{oil} (l s^{-1})
7500	2.5	0.38	0.115	0.0030
	5	0.38	0.112	0.0059
	7.5	0.38	0.109	0.0088
	10	0.38	0.106	0.0118
	12.5	0.38	0.103	0.0147
	15	0.38	0.100	0.0177
10 000	2.5	0.50	0.153	0.0039
	5	0.50	0.149	0.0079
	7.5	0.50	0.145	0.0118
	10	0.50	0.141	0.0157
	12.5	0.50	0.137	0.0196
	15	0.50	0.134	0.0236
12 500	2.5	0.63	0.191	0.0049
	5	0.63	0.187	0.0098
	7.5	0.63	0.182	0.0147
	10	0.63	0.177	0.0196
	12.5	0.63	0.172	0.0245
	15	0.63	0.167	0.0295
15 000	2.5	0.75	0.230	0.0059
	5	0.75	0.224	0.0118
	7.5	0.75	0.218	0.0177
	10	0.75	0.212	0.0236
	12.5	0.75	0.206	0.0295
	15	0.75	0.200	0.0353

hydrodynamic conditions. The reference situation for each flow rate is the single-phase flow, for which the flow pattern and the turbulent field have been studied in detail in previous work (Mokrani et al., 1995, submitted for publication). Table 2 summarises the operating conditions. All experiments were performed at room temperature (18–20 °C).

4.2. Mean and maximum diameter

Proportionality between the Sauter mean diameter, d_{32}, and the maximum diameter of the drops, d_{max}, is often hypothesised (Sprow, 1967; Pacek et al., 1998) but not so often examined experimentally. This criterion is very important in using the breakup models resulting from the theories of Hinze and Kolmogorov, which, as it was mentioned above, predict the size of the largest drop viable in the flow, precisely the value of d_{max}. The experimental results (Fig. 8) reveal that the diameters d_{32} and d_{max} are actually correlated according to the linear relation

$$d_{32} = C_{10} d_{max} \tag{29}$$

The value of 0.48 for C_{10} (Fig. 8) is within the range of the values found in the literature: between 0.38 and 0.7 for agitated tanks and bent tubes equipped with a static mixer (Zhou and Kresta, 1998).

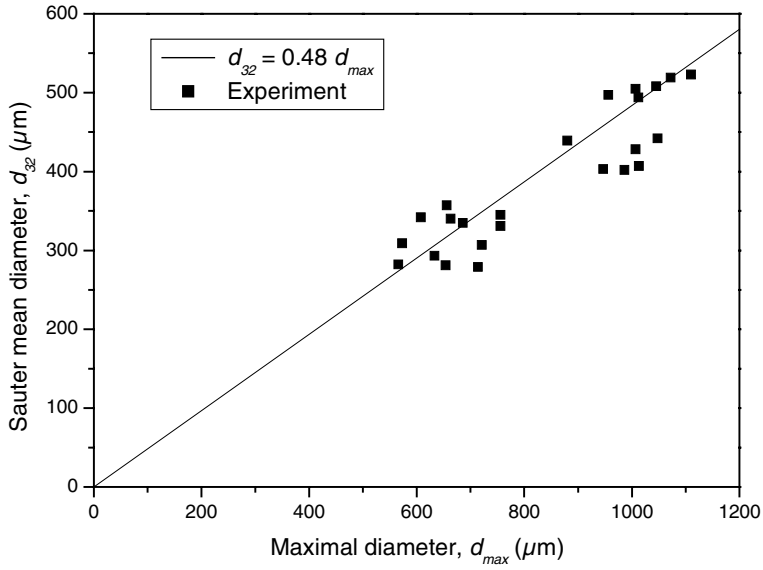

Fig. 8. Sauter mean diameter versus maximal diameter of droplets.

4.3. Sauter mean diameter as a function of oil fraction

For a given overall flow rate, i.e. a given local velocity for the continuous phase, Fig. 9 shows that changes in the volume fraction produce a slight increase in the Sauter diameter. Nevertheless,

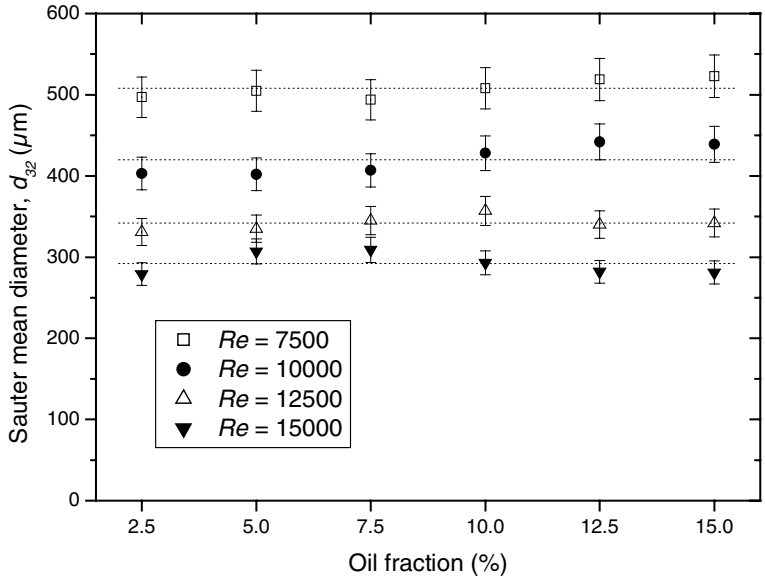

Fig. 9. Sauter mean diameter versus oil volume fraction for different flow Reynolds numbers.

the observed variations are within the confidence interval, about 5%, as mentioned in Section 3.6, allowing the conclusion that d_{32} is independent of the volume fraction in the range 0–15%.

4.4. Sauter diameter as a function of Weber and Reynolds numbers

The average drop diameter depends strongly on the hydrodynamic conditions through the energy dissipation rate. In the present case, the Kolmogorov length (about 20–50 μm) is much less than the drop size, so that the typical drop size is expected to be proportional to $We^{-0.6}$ (Sprow, 1967; Walstra, 1993). The mean diameter is obtained by the linear relationship that exists between d_{32} and $d_{\max}$. The HEV measurements plotted in Fig. 10 show fairly good agreement with this theoretical slope of −0.6,

$$\frac{d_{32}}{D} = C_{11} We^{-0.6} \tag{30}$$

with $C_{11} = 0.57$, demonstrating that turbulent disruption governs the emulsification mechanism.

Experimental results are also compared with the Streif formula (Eq. (16)) in Fig. 11, with the same fit level as for the general breakup model. In the present study, the constant of best fit is 0.087 (smaller than 0.2), suggesting that in similar conditions the Sauter diameter is smaller in the HEV than in the classical static mixers. This feature will be confirmed by the analysis of the energy utilisation efficiency of this device.

4.5. Dispersion factor

The dispersion factor is defined as the ratio between the standard deviation, SD, and the arithmetic average diameter, d_a:

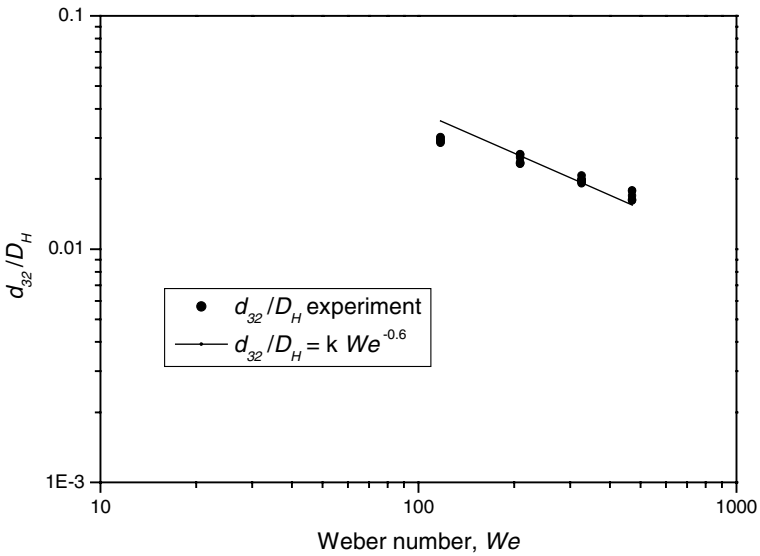

Fig. 10. Comparison of experimental Sauter diameter and predicted Sauter diameter by the general break up model.

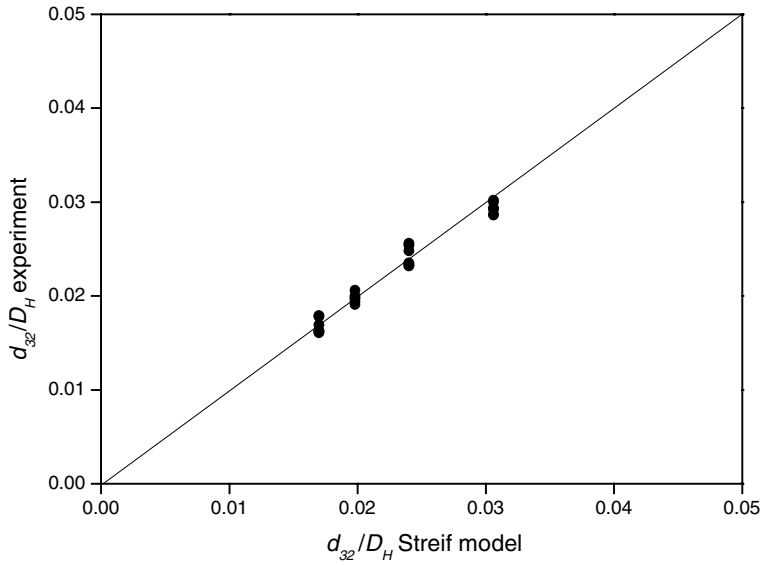

Fig. 11. Comparison of experimental Sauter diameter and predicted Sauter diameter by the Streif model.

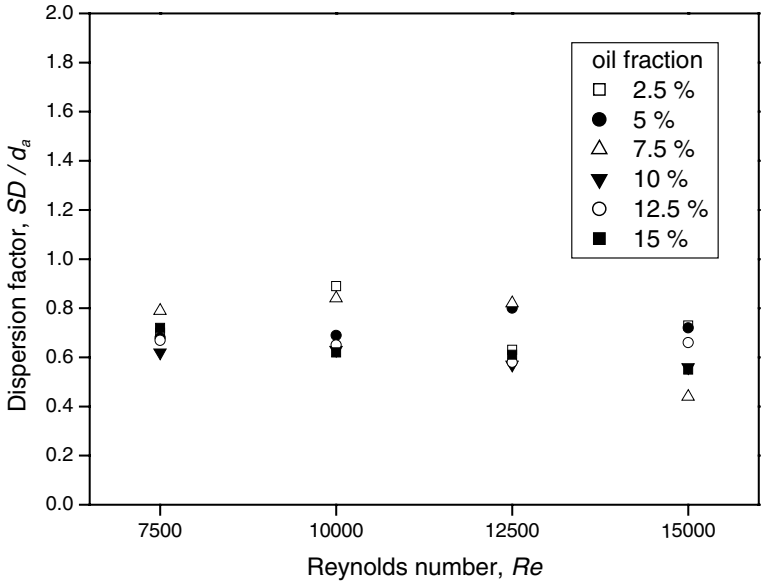

Fig. 12. Dispersion factor in the drop size distribution as a function of Reynolds number.

$$\text{dispersion factor} = \frac{\text{SD}}{d_{\text{a}}} \tag{31}$$

The dispersion factor is plotted in Fig. 12 as a function of the flow rate and the oil concentration. Few authors have focused on the distribution function, and moreover the definition of a

spread characteristic is yet not generally agreed upon, making any comparison difficult. Morançais (1997) has found a similar dispersion factor for static mixers in the range 0.5–1. Nevertheless, it is clear from Fig. 12 that the dispersion factor is independent of the operating conditions: the dispersion factor is in the range 0.5–0.9 and is centred around 0.7.

The method proposed by Schwarz and Bezemer (1956), useful for extrapolation, was applied to fit the present data. The cumulative volume $V\%$ of the distribution function is modelled, using a typical constant a:

$$\ln V\% = \ln 100 + \frac{a}{d_{\max}} - \frac{a}{d} \tag{32}$$

Fig. 13 shows a plot based on Eq. (32) for an emulsion of oil fraction 5% obtained at various Reynolds numbers. For each Reynolds number the data fits quite well the linear relationship between $\ln V\%$ and $1/d$, showing that Schwarz and Bezemer model represents the droplet size distribution in HEV. Table 3 summarises the values of the parameter a of the Schwarz and Bezemer model obtained from Fig. 13.

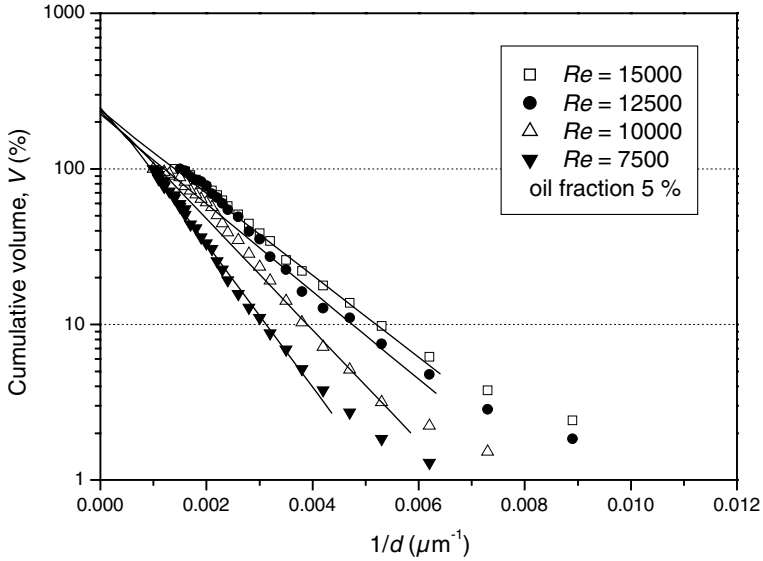

Fig. 13. Experimental drop size distributions modelled using the analysis of Schwarz and Bezemer.

Table 3
Parameters and results of the Schwarz–Bezemer equation for $\Phi = 5\%$

Re	a (μm)	$d_{32\ cal}$ (μm)	$d_{32\ exp}$ (μm)	$d_{32\ exp}/d_{32\ cal}$
7500	1116	526	547	1.04
10 000	864	408	430	1.05
12 500	730	342	362	1.06
15 000	616	320	344	1.07

An interesting feature of Fig. 13 is that the various sets of data extrapolate to nearly the same intercept. This indicates that the value of $a/d_{\max}$ is a constant (equal to 1.08) independent of the operating conditions. This is of consequence since all the usual average diameters are functions of this ratio. For example, the Sauter mean diameter, d_{32}, can be expressed in terms of the parameters of the Schwarz–Bezemer equation as:

$$d_{32} = \frac{a}{1 + \frac{a}{d_{\max}}} \tag{33}$$

Any d_{pq} moment of the distribution can then be calculated from the following expression:

$$d_{pq} = a \left[\frac{(3-p)! \sum_{k=0}^{3-p} \frac{1}{k!} \left(\frac{a}{d_{\max}} \right)^k}{(3-q)! \sum_{k=0}^{3-q} \frac{1}{k!} \left(\frac{a}{d_{\max}} \right)^k} \right] p - q \tag{34}$$

for $p = 1, 2, 3$; $q = 0, 1, 2$; and $p > q$ (Sprow, 1967).

Table 3 shows $d_{32\ \mathrm{cal.}}$ and $d_{32\ \mathrm{exp.}}$, the Sauter mean diameters respectively calculated with Eq. (33) and obtained experimentally. The ratio between these two variables highlights the high precision of the Schwarz–Bezemer equation in predicting the Sauter mean diameter: predicted values lie between 4% and 7% of the experimental values.

From Eq. (34), for a given system in which $a/d_{\max}$ is independent of the operating conditions, the average droplet sizes are directly proportional to a and thus to $d_{\max}$:

$$d_{pq} = C_{12} d_{\max} \tag{35}$$

and the constant C_{12} can be evaluated for various values of p and q. It has been accepted by most workers that Eq. (35) is valid for d_{32} for liquid–liquid dispersed systems (Calabrese et al., 1986) and also for gas–liquid dispersions (Parthasarathy and Ahmed, 1994; Barigou and Greaves, 1992). Occasionally, the constant of proportionality in Eq. (35) has been estimated around 0.6 for d_{32} (Baldyga et al., 1997).

5. Discussion

5.1. Energy cost

The energy consumed in this experiment is the external pumping power necessary to propel the fluids through the static mixer. This energy is dissipated through turbulent fluctuations. Most of the energy extracted from the main stream results in a pressure drop and is converted into heat. A small part is devoted to the potential surface energy due to the creation of new interfacial area during emulsification:

$$E_S = \frac{\sigma A}{\rho} \tag{36}$$

This energy is generally a small fraction of the global energy involved. Fig. 14 shows an estimate of the specific internal energy and of the mechanical specific energy ($J\,kg^{-1}$) as a function of mean velocity. The ratio of the internal energy to the available mechanical energy is shown in Fig. 15.

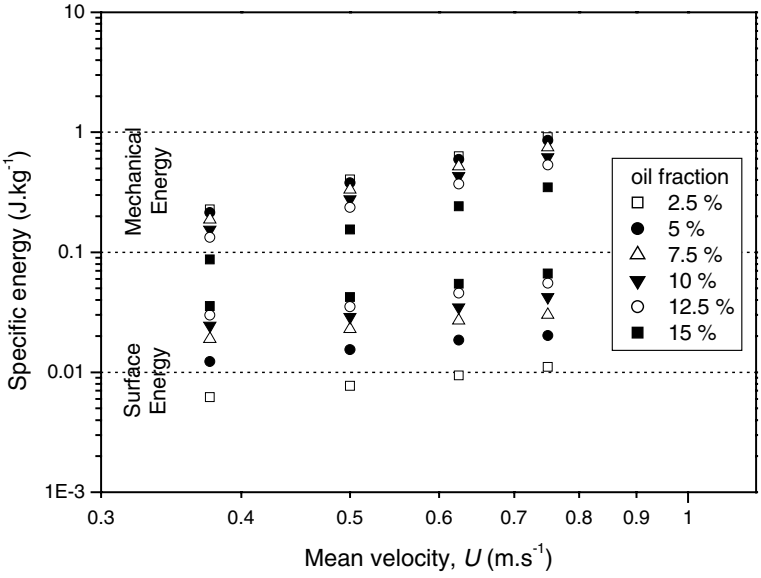

Fig. 14. Energy balance for the HEV mixer in the emulsification process.

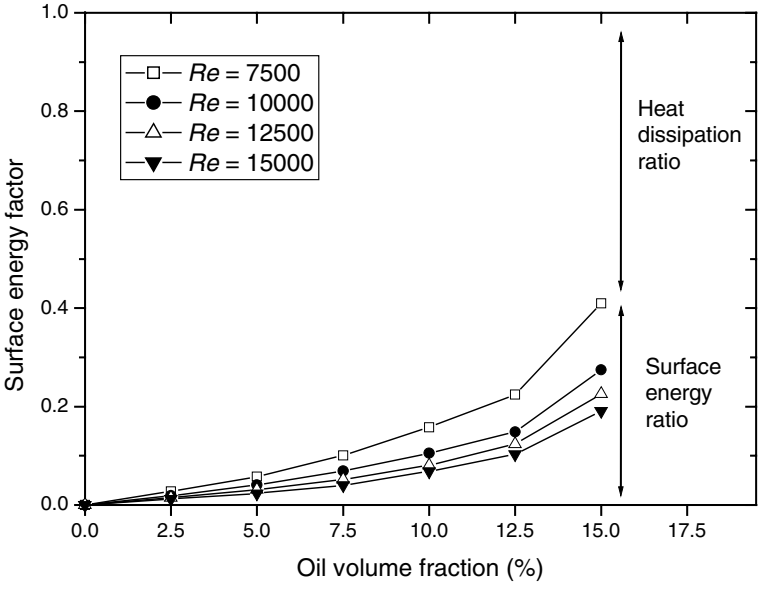

Fig. 15. Surface energy fraction as a function of oil volume fraction.

The mean energy dissipation rate is computed from the total power consumption for a unit of mass of the processed fluid:

$$\overline{\varepsilon} = \frac{Q\Delta P}{\rho V} = \frac{U\Delta P}{\rho L} \quad (\mathrm{W\,kg^{-1}}) \tag{37}$$

The specific energy is obtained by integration over the residence time L/U:

$$E = \frac{\Delta P}{\rho} \quad (\mathrm{J\,kg^{-1}}) \tag{38}$$

The pressure drop values in the test section are presented in Fig. 16 as a function of the global flow rate. The parabolic shape of the curves for a given hold-up is in agreement with the general behaviour of turbulent flows. Nevertheless, all the curves lie significantly above the theoretical curve for a simple smooth duct of the same hydraulic diameter.

The z factor, defined as the pressure drop ratio between the HEV and the simple duct

$$z = \left(\frac{\Delta P_{\mathrm{HEV}}}{\Delta P_{\mathrm{Duct}}}\right)_{Q,\alpha} \tag{39}$$

as plotted in Fig. 17, shows that the dissipative efficiency provided by the vortex generators is up to an eight-fold increase and is independent of the flow rate.

Moreover, the pressure drop measurements show an important decrease by increasing the oil volume concentration. This can be explained by the damping of turbulence occurring near the contact surface between the two phases, observed even at very low dispersed-phase concentration. The damping factor (Fig. 18) is calculated with reference to the single-phase flow in the HEV. From the plot of Fig. 18, one can deduce an estimation of the z factor:

$$z = 7.9(1 - 28.7\Phi^2) \tag{40}$$

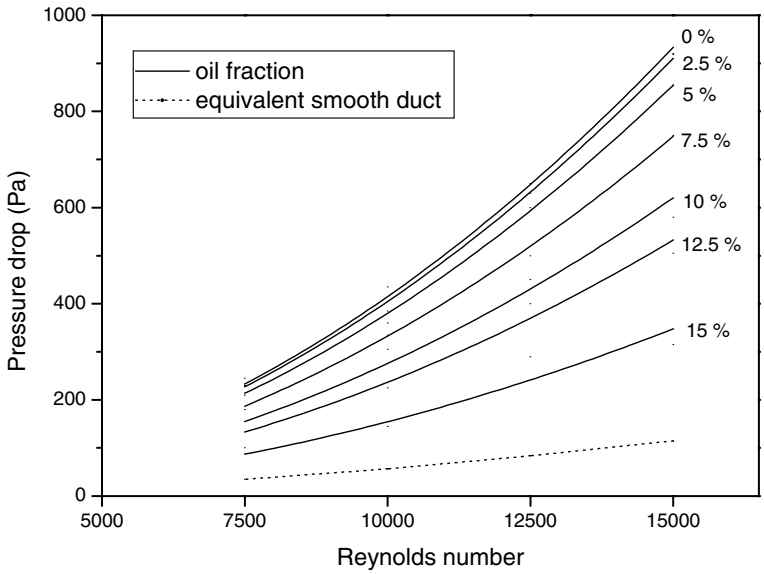

Fig. 16. Dimensional pressure drop in the mixer versus flow rate.

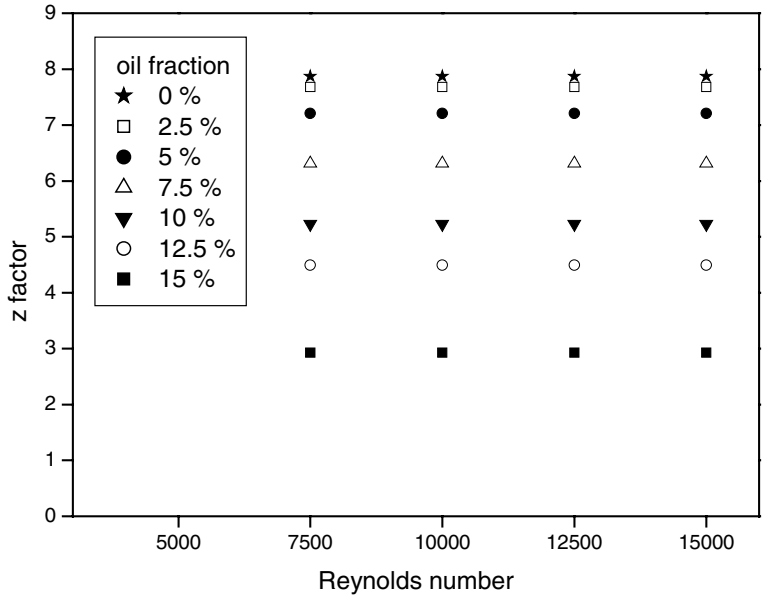

Fig. 17. z factor versus Reynolds number.

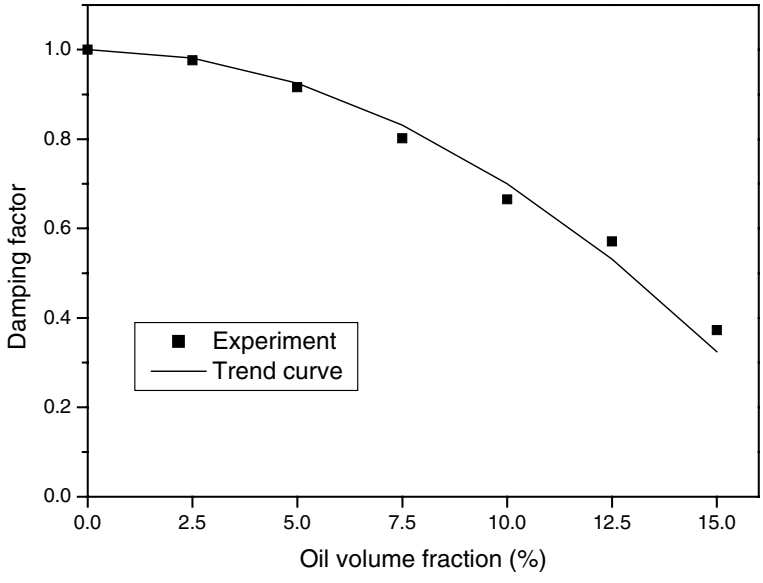

Fig. 18. Damping factor versus hold-up.

5.2. *Efficiency*

To assess the efficiency of HEV as an emulsifier, we compare its energy cost with that of existing devices. HEV experimental data are compared with those reported by previous investigators. In

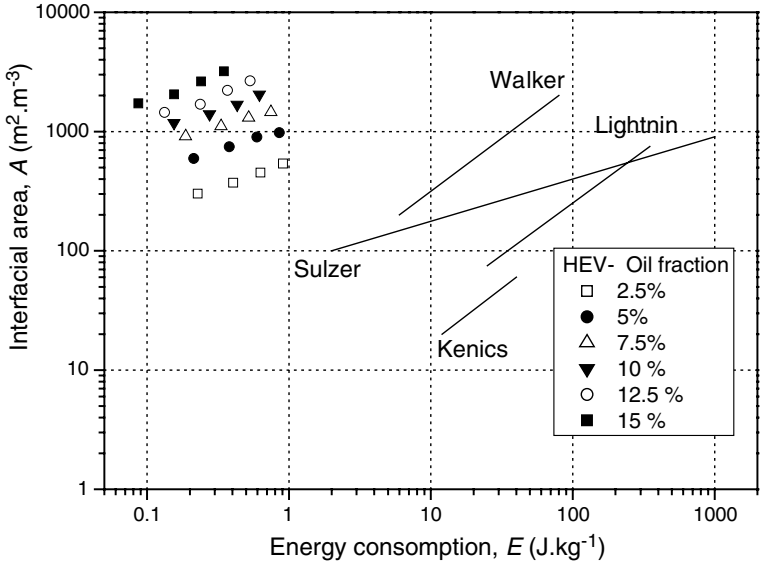

Fig. 19. Comparison of the energy consumption of HEV with classical static mixers (data from Al Taweel and Chen, 1996).

Fig. 19, the energy spent in phase dispersion is correlated with the interfacial area generated by each system. The contact area is readily given by the Sauter diameter:

$$A = \frac{6\Phi}{d_{32}} \tag{41}$$

Fig. 19 compares the measured interfacial area as a function of the turbulent dissipation rate in the HEV and other commercially available systems (Al Taweel and Chen, 1996). The working zone of the HEV mixer is in the small-energy range (between 0.1 and 1 $J\,kg^{-1}$) for a typical interfacial area of 300–3000 $m^2\,m^{-3}$. This shows a good efficiency for the dispersion of immiscible liquid: up to 1000 times decrease in energy consumption in the range of interfacial area around 1000 $m^2\,m^{-3}$.

The very low energy level, and the relatively high contact obtained without any surfactant, show that HEV mixers have good potential in industrial applications.

A correlation between the interfacial area, A and the consumed energy, E can be found from Eq. (41), replacing d_{32} by Eq. (30) and substituting We by the definition in Eq. (13) which gives

$$A = \frac{6 \cdot \Phi}{C_{11} \cdot D} \left(\frac{\rho \cdot U^2 \cdot D}{\sigma} \right)^{0.6}$$

the U^2 expression can be calculated by the Eqs. (37)–(40), so that

$$U^2 = \frac{2 \cdot D \cdot E}{f \cdot L \cdot z(\Phi)}$$

leads to:

$$A = \frac{6 \cdot \Phi}{C_{11}} \left[\frac{2\rho}{7.9(1 - 28.7\Phi^2) \cdot \sigma \cdot f \cdot L} \right]^{0.6} \cdot D^{0.2} \cdot E^{0.6} \tag{42}$$

5.3. Equilibrium size

Mokrani et al. (submitted for publication) made an extensive analysis of a large amount of laser Doppler velocimetry data. The objective of this analysis was to describe the turbulent energy dissipation distribution in the HEV geometry. The equation suggested for evaluation of the energy dissipation was

$$\varepsilon \approx C_{13} \frac{\left(\frac{3}{2}u'^2\right)^{3/2}}{\Lambda} \tag{43}$$

where C_{13} is a constant, u' the fluctuating part of the axial velocity and Λ the macro-scale of turbulent fluctuations. The value of the empirical constant C_{13} has been the subject of many studies. Additional analysis was necessary to evaluate C_{13} in the specific conditions of the flow generated in the HEV. The analysis was based on a comparison of the HEV results with experimental results of energy dissipation obtained by Lawn (1971) in a straight circular tube.

The macro-scale Λ was derived from the temporal autocorrelation function of the instantaneous velocity. An appropriate convection velocity was calculated by using a generalised Taylor hypothesis. Wu and Patterson (1989) have already obtained satisfactory results using this method. Fig. 20 shows the evolution of $\varepsilon_{max}/\overline{\varepsilon}$ along the HEV mixer obtained from the measurements of Mokrani et al. (submitted for publication).

It is well established that in a given system, where some disruptions of the droplets occur, an equilibrium size is reached, that fixes the maximum drop size that can resist the turbulent forces. It

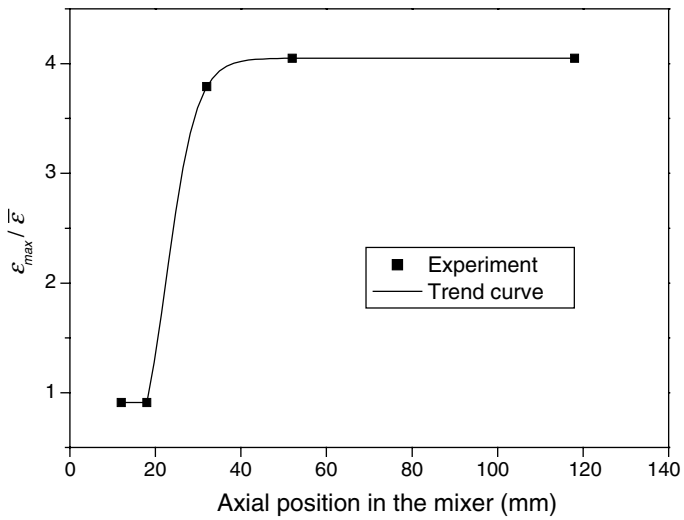

Fig. 20. Variation of $\varepsilon_{max}/\overline{\varepsilon}$ along the static mixer.

is understandable that the successive divisions that lead to this equilibrium size will need a "certain" time. If this time is longer than the residence time, the droplets obtained will be coarser than the predicted size, and thus the system could be optimised by increasing the residence time, for instance by adding another mixing element. The time-scale estimates proposed by some authors (Davies, 1985; Hesketh et al., 1991) suggest that the minimal residence time for optimal division would be between 1.5 and 10 s. The characteristic time for a droplet break up is estimated at about 1 μs, and a sufficient number of divisions must take place.

To analyse these features in the present system, Fig. 21 compares the experimental maximum drop size to the predicted one with the Hinze theory, using a critical Weber number of the order of unity:

$$d_{\max} = \left(\frac{We_{\text{crit}}}{2}\right)^{0.6} \left(\frac{\sigma^{0.6}}{\rho_c^{0.4}\rho_d^{0.2}}\right) \varepsilon^{-0.4} \tag{44}$$

The predicted maximum values with the mean turbulence dissipation rate are slightly higher than the measured values. This could mean that the equilibrium diameter is reached and that the HEV mixer is long enough. Nevertheless, considering the local nature of the dissipation rate and that the maximum "surviving" drop size in the flow is governed by the highest turbulence intensity, the maximum diameter is also computed from the maximum ε value in the middle of the mixer. From this point of view, the equilibrium should be better achieved by the addition of one or two baffle arrays. In other words, it can be concluded from this plot that the actual drop size is controlled by a dissipation rate somewhere between the mean and the maximum local value. The non-uniformity of the dissipation field may explain the discrepancy between various flow configurations, as far as the global behaviour cannot be "linearly" deduced from the local analysis.

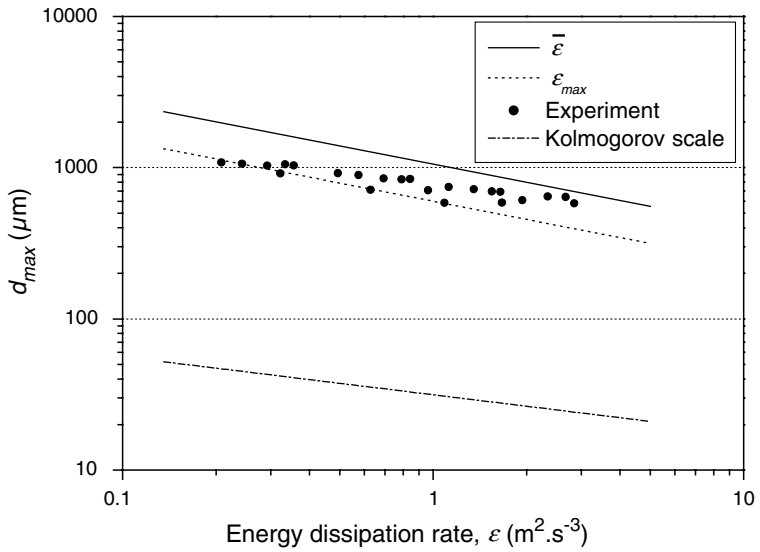

Fig. 21. Predicted equilibrium diameter (Hesketh theory).

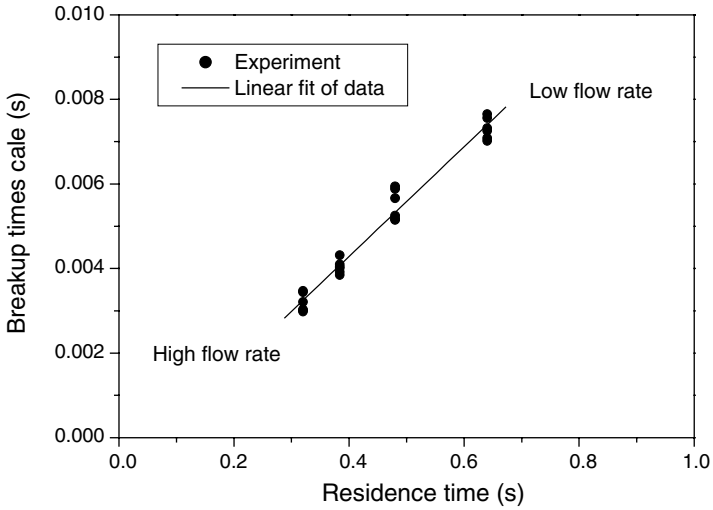

Fig. 22. Estimation of the division time scale in the HEV mixer.

5.4. Time scales

According to Hesketh et al. (1991), the break up time scale is linked to the second order natural mode of oscillation of the sphere (providing the largest amplitude):

$$f_2 = \left(\frac{2\sigma}{\pi^2 \rho_c d^3}\right)^{0.5} \left(\frac{24}{3\frac{\rho_d}{\rho_c} + 2}\right)^{0.5} \tag{45}$$

This disruption time (the inverse of f_2) was calculated for each run and is plotted versus the corresponding residence time in Fig. 22. The constant slope of the curve indicates that the number of divisions is independent of the operating conditions.

6. Conclusions

Formation of droplets in the turbulent flow of two immiscible fluids in a HEV mixer was studied. The mixing mechanism is by generation of a cascade of longitudinal vortices formed behind the rows of baffles fixed in a straight tube of circular cross-section. Vortices generate extra shear in the flow and hence increase the turbulent energy dissipation which contributes directly to droplet break-up.

The main features of droplet formation are experimentally investigated and compared with models. Experiments have been carried out in low hold-up range (0–15%) and the linear relation between the Sauter mean diameter and maximum droplet diameter is verified. The correlation constant is found to be 0.48. The variation of the Sauter mean diameter with the volume fraction of the dispersed phase has also been investigated. Experimentally it has been shown that for the range of 0–15% volume fraction studied here, the Sauter diameter is independent from the volume

fraction of the dispersed phase. This is not the case for the effect of Weber number on the Sauter mean diameter, where it is found that this diameter varies with −0.6 power of the Weber number, demonstrating that the dominating mechanism of emulsification is by turbulent disruption.

The Sauter mean diameter obtained with the present mixer was also compared with Streif formula. It was revealed that for similar conditions, the HEV mixer provides smaller Sauter diameters than the classical static mixers.

The size distribution of the droplets obtained with HEV was modelled according to the method proposed by Schwarz and Bezemer (1956). In a log-linear coordinates system the data showed a linear relation between the cumulative volume (in%) of droplet diameters and the inverse of the bounding diameter d, showing that the Schwarz–Bezemer model is verified here. This model also showed that the ratio $a/d_{\max}$ (where a is the characteristic diameter corresponding to the maximum of the distribution function) is independent from the operating conditions.

The overall energy cost of the HEV mixer was another aspect studied in this work. Experimental pressure drop measurements showed that the vortex generators increase the dissipative efficiency by as high as eight-folds, and that this increase is independent from the flow rate. The energy consumption for generation of interfacial area with the HEV mixer was compared with some common static mixers. In some range of interfacial area (1000 $m^2\,m^{-3}$) it was shown that HEV is 1000 times more energy efficient than other mixers.

Acknowledgements

The authors thank Jack Legrand and Jean-Michel Rosant for their help in implementing the micro-encapsulation technique. The authors also thank Pascal Dupont for illuminating discussions.

References

Al Taweel, A.M., Chen, C., 1996. A novel static mixer for the effective dispersion of immiscible liquids. Transactions of the Institution of Chemical Engineers 74 (Part A), 445–450.

Arai, K., Konno, M., Matunaga, Y., 1977. Effect of dispersed-phase viscosity on the maximum stable drop size for breakup in turbulent flow. Journal of Chemical Engineering of Japan 10, 325–330.

Baldyga, J., Podgorska, W., Smit, L., 1997. Turbulent dispersion of drops in intermittent turbulence. Récent Progrès en Génie des Procédés 11, 247.

Barigou, M., Greaves, M., 1992. Bubble size distribution in a mechanically agitated gas–liquid contactor. Chemical Engineering Science 47, 2009.

Berkman, P.D., Calabrese, R.V., 1988. Dispersion of viscous liquids by turbulent flow in a static mixer. AIChE Journal 34, 602–609.

Calabrese, R.V., Chang, T.P.K., Dang, P.T., 1986. Drop breakup in turbulent stirred-tank contactors. AIChE Journal 32, 657–666.

Clark, M.M., 1988. Drop breakup in a turbulent flow-I. Conceptual and modeling considerations. Chemical Engineering Science 43, 671–679.

Coulaloglou, C.A., Tavlarides, L.L., 1976. Drop size distributions and coalescence frequencies of liquid–liquid dispersions in flow vessels. AIChE Journal 22, 289–297.

Davies, J.T., 1985. Drop sizes of emulsions related to turbulent energy dissipation rates. Chemical Engineering Science 40, 839–842.

Grace, H.P., 1982. Dispersion phenomena in high viscosity immiscible fluid systems and application of static mixers as dispersion devices in such systems. Chemical Engineering Communications 14, 225–277.

Hinze, J.O., 1955. Fundamentals of the hydrodynamic mechanism of splitting in dispersion processes. AIChE Journal 1, 289–295.

Hesketh, R.P., Etchells, A.W., Russell, T.W.F., 1991. Bubble breakage in pipeline flow. Chemical Engineering Science 46, 1–9.

Lagisetty, J.S., Das, P.K., Kumar, R., 1986. Breakage of viscous and non-Newtonian drops in stirred dispersion. Chemical Engineering Science 41, 65–72.

Lawn, C.J., 1971. The determination of the rate of dissipation in turbulent flow. Journal of Fluid Mechanics 48, 477–505.

Middleman, S., 1974. Drop size distributions produced by turbulent pipe flow of immiscible fluids through a static mixer. Industrial and Engineering Chemistry Process Design and Development 13, 78–83.

Mokrani, A., Castelain, C., Peerhossaini, H., 1995. Experimental study of the turbulent flow inside a motionless on-line mixer. In: Phillips, C.H. (Ed.), Process intensification for the chemical industry. BHR-Ltd, pp. 115–124.

Mokrani, A., Castelain, C., Peerhossaini, H., 2002. Experimental study of the influence of the rows of vortex generators on turbulence structure in a tube. Experiments in Fluids, submitted for publication.

Morançais, P., 1997. Etude de la formation des émulsions dans des mélangeurs statiques. Application aux procédés de microencapsulation par polymérisation interfaciale, PhD Thesis, Université de Nantes, France.

Pacek, A.W., Man, C.C., Nienow, W., 1998. On the Sauter mean diameter and size distributions in turbulent liquid/liquid dispersions in a stirred vessel. Chemical Engineering Science 53, 2005–2011.

Parthasarathy, R., Ahmed, N., 1994. Sauter mean and maximum bubble diameters in aerated stirred vessels. Transactions of the Institution of Chemical Engineers 72 (Part A), 565.

Pichot, G., 1984. Propriétés de transport des suspensions industrielles appliquées au transport des bruts lourds émulsionnés, PhD Thesis, ENSM-Université de Nantes, France.

Poncelet, D., Neufeld, R.J., 1996. Fundamentals of dispersion in encapsulation technology. In: Wijffels, R.H., Buitelaar, R.M., Bucke, C., Tramper, J. (Eds.), Immobilized Cells: Basics and applications. Elsevier Science B.V., pp. 47–54.

Schubert, H., Armbruster, H., 1992. Principles of formation and stability of emulsions. International Chemical Engineering 32, 14–28.

Schwarz, N., Bezemer, C., 1956. A new equation for the size distribution of emulsion particles. I. Derivation and application to experimental data. Kolloid-zeitschrift 146, 139–145.

Shinnar, R., 1961. On the behaviour of liquid dispersions in mixing vessels. Journal of Fluid Mechanics 10, 259–275.

Sprow, F.B., 1967. Distribution of drop sizes produced in turbulent liquid–liquid dispersion. Chemical Engineering Science 22, 435–442.

Streif, F., 1977. In-line dispersion and mass transfer using static mixing equipment. Sulzer Technical Review 3, 108–113.

Taylor, G.I., 1932. The viscosity of a fluid containing small drops of another fluid. Proc. Roy. Soc. 138, 41–48.

Taylor, G.I., 1934. The formation of emulsions in definable fields of flow. Proc. Roy. Soc. 146, 501.

Walstra, P., 1993. Principles of emulsion formation. Chemical Engineering Science 48, 333–349.

Wang, C.Y., Calabrese, R.V., 1986. Drop break-up in turbulent stirred tank contactors. Part 2: Relative influence of viscosity and interfacial tension. AIChE Journal 32, 667–676.

Wu, H., Patterson, G.K., 1989. Laser-Doppler measurements of turbulent flow parameters in a stirred mixer. Chemical Engineering Science 44, 2204–2221.

Zhou, G., Kresta, S.M., 1998. Correlation of mean drop size and minimum drop size with the turbulence energy dissipation and the flow in an agitated tank. Chemical Engineering Science 53, 2063–2079.